



Enhancement of dielectric properties by modulating electroactive β -phase of copper doped nickel oxide nanoparticles incorporated thin film

Somen Biswas^{1,2} · Indrajit Mondal¹ · Piyali Halder¹ · Souvik Sau^{1,2} · Manisha Kundu^{1,3} · Dheeraj Mondal⁴ · Anagha Ghosh⁶ · Biplab Kumar Paul⁵ · Sukhen Das¹

Received: 22 December 2023 / Accepted: 11 April 2024 / Published online: 11 May 2024
© The Polymer Society, Taipei 2024

Abstract

Polymer nanocomposites (PNCs), exhibiting enhanced physical properties, are emerging as innovative functional materials due to their versatile characteristics suitable for various technological applications. Composite films comprising 0.1% copper (Cu) doped Nickel oxide (NiO) [CNO1 (350)] nanoflakes calcined at 350 °C embedded in Poly (vinylidene fluoride) (PVDF) polymer were prepared using the solution casting method. The influence of CNO1 (350) filler incorporation on the structure and morphology of the composite films was scrutinized through X-ray diffraction (XRD), Fourier-transformed infrared spectroscopy (FTIR), and Field Emission Scanning Electron Microscopy (FESEM). Results unveiled a direct correlation between CNO1 (350) filler concentration and the crystallinity, β -phase content, and morphology of the composite films, attributed to heterogeneous nucleation. Room temperature electrical measurements indicated dielectric constants reaching more than six times at 40 Hz and a conductivity increase exceeding two orders of magnitude, with a percolation threshold identified around 25wt% of CNO1 (350) filler content. The observed outcomes are elucidated through Maxwell–Wagner–Sillars interfacial polarization occurring at the interface of CNO1 (350) and the insulating polymer matrix. This elucidation involves the development of a conductive network and the establishment of a micro-capacitive structure within the PVDF thin films modified with CNO1 (350).

Keywords Doped electroactive polymer · Doped transition metal oxide · β -phase enhancement · Dielectric property · Solution casting technique

Introduction

Electroactive polymers have garnered a lot of attention recently, as they offer so much promise for use in biomedical devices, sensors, electrochemical devices, energy harvesters, actuators, and so on [1–3]. Additionally, high dielectric polymer nanocomposites with low tangent loss materials have garnered significant attention in recent years due to their promising applications in a wide range of fields such as electronics, energy storage, and telecommunications [3–5]. The quest for materials with enhanced dielectric properties, characterized by high permittivity and low loss tangent, has driven extensive research efforts toward the development of advanced nanocomposite systems. These materials offer the potential to revolutionize various technologies by improving device performance, reducing energy consumption, and enabling miniaturization [6, 7]. In this context, poly (vinylidene fluoride) (PVDF) and its copolymers, such as poly (vinylidene fluoride-trifluoro

✉ Biplab Kumar Paul
destinationbiplab@gmail.com

✉ Sukhen Das
sdasphysics@gmail.com

¹ Department of Physics, Jadavpur University, Kolkata 700032, India

² Department of Physics, Bangabasi College, Kolkata 700009, India

³ Department of Physics, Jogamaya Devi College, Kolkata 700026, India

⁴ Department of Physics, Nabagram Hiralal Paul College, Hooghly 712246, India

⁵ University of Engineering and Management, Kolkata 700160, India

⁶ Central Glass and Ceramic Research Institute, Kolkata 700032, India

ethylene) [P(VDF-TrFE)] and poly (vinylidene fluoride-co-hexafluoropropylene) [P(VDF-HFP)], stand out as versatile candidates with remarkable electroactive properties [8–11]. PVDF ($[\text{CH}_2\text{-CF}_2]_n$) is an economical and flexible fluoropolymer that has gained significant interest owing to its diverse applications in non-volatile memories in microelectronics, thin-film transistors, magnetostriction, piezoelectric nanogenerators, high-capacity charge storage capacitors, pulsed lasers, and electrostriction for artificial muscles and beyond [1, 8–11]. Commercially available PVDF polymer exhibits five different crystalline phases, including α , β , γ , δ and ϵ . The most prevalent and thermodynamically stable phase at standard temperature and pressure is the non-polar phase. Due to their superior piezoelectric, ferroelectric, and pyroelectric properties [9, 10, 12–14], the polar and phases of PVDF, which are defined by their orthorhombic unit cell structures with TTT (all trans) and 3TG3TG conformation, have drawn significant attention nowadays [15]. Numerous processes, including stretching [16], quenching [17], uniaxial or biaxial drawing of -PVDF films [18–20], simultaneous poling, phase-inversion process [4, 10], multi-step processing [21], and supercritical carbon dioxide processing [22], have been developed in an attempt to enhance the electroactive-phase concentration in PVDF [10]. Incorporation of nano-or submicron-sized filler materials, such as graphene [13, 20], ferrites [3, 23, 24], inorganic salts [25], clays [26], carbon nanotubes [27, 28], ceramics [29–31], metals [32, 33], and metal oxides [34, 35] are another effective strategy for the successful enhancement in β -phase [5, 6, 12–14, 36–40]. The β -phase of PVDF serves as a versatile platform for the development of high dielectric and low tangent loss materials, offering a balance between enhanced polarization, reduced energy dissipation, stable electrical performance, and mechanical flexibility [10]. Its unique properties make it well-suited for a wide range of applications in electronics, telecommunications, energy storage, and beyond [41, 42]. The addition of these nanofillers, results in an improved physicochemical profile of the polymer without compromising its flexibility [43].

The integration of metal oxide nanoparticles (e.g., ZnMnO₃ [1], MoO₃ [2], ZrO₂ [5], ZnO [40, 44], Mg-Doped Nickel Oxide [45], Fe-ZnO [46], CoCr₂O₄ quantum dots [47], Cu-doped α -MnO₂ [48], PVDF/MgO [49], BaTiO₃ [50] with tailored dielectric properties into polymer matrices, particularly polymeric matrices such as polyvinylidene fluoride (PVDF), has emerged as a promising strategy to achieve superior dielectric characteristics [51, 52]. By carefully engineering the composition and morphology of different nanocomposites like (Al/ β -SiCw/PVDF [11], PVDF/BaTiO₃/NiO [50], PMMA/PVDF Blend by Incorporation of Ni/ZnO [53], PVDF/BaTiO₃/NiO [54], researchers aim to exploit synergistic effects between the polymer matrix and the nanoparticles to optimize dielectric properties while

mitigating loss mechanisms. This introduction provides a foundation for understanding the significance of high dielectric polymer nanocomposites with low tangent loss materials and sets the stage for exploring the latest advancements and challenges in this exciting field of research (ref from existing ref). In this context, copper doped Nickel oxide nanoparticles (CNO) have gained prominence as cost-effective fillers known to notably enhance the electrical properties of PVDF [36, 39]. Prior investigations have demonstrated a remarkable increase in the (~ 63) within copper doped Nickel oxide/PVDF nanocomposite films.

In our earlier work [39] we extensively investigated the impact of calcination on various physicochemical properties on divalent (Cu^{2+}) metal cation doped transition metal oxide nanoparticles. This study presents a modified chemical synthesis method for copper doped nickel oxide nanoparticles [CNO1 (350)] [39] and their incorporation into the host polymer (PVDF) matrix. Thorough analyses of the various structural and physicochemical properties of CNO-loaded PVDF films have been conducted. Furthermore, we investigate the effect of CNO1 (350) on the nucleation of the electroactive β -phase in PVDF and provide insights into the significant enhancement of the β -phase fraction from a physicochemical perspective. Finally, the electrical properties of all samples are recorded.

Experimental section

Materials

In this study, to synthesize copper doped nickel oxide incorporated PVDF nanocomposite thin film, the following analytical grade chemicals were used: Poly (vinylidene fluoride) (PVDF) (Sigma Aldrich, M_w : 180 000 GPC, M_n : 71 000), Dimethylformamide (Merck, India), polyvinyl alcohol (PVA), Nickel acetate tetra-hydrate ($\text{C}_4\text{H}_6\text{NiO}_4 \cdot 4\text{H}_2\text{O}$, 98% Sigma-Aldrich); Copper acetate di-hydrate ($\text{Cu}(\text{CH}_3\text{COO})_2 \cdot 2\text{H}_2\text{O}$, 98% Sigma-Aldrich) and potassium hydroxide pellet (KOH, 99.99% Sigma-Aldrich). The aforementioned chemicals were used without further purification. Throughout the synthesis procedure, absolute ethanol (HPLC grade) and double deionized water were used to synthesize the material.

Synthesis technique

The nanoparticle was prepared through modified chemical synthesis process followed by post-annealing. Then incorporated into the polymer matrix using solution-casting method. The detailed preparation procedure was noted below.

Firstly, to prepare 0.1% copper-doped nickel oxide, Nickel acetate tetra-hydrate ($\text{C}_4\text{H}_6\text{NiO}_4 \cdot 4\text{H}_2\text{O}$) and Copper acetate di-hydrate ($\text{Cu}(\text{CH}_3\text{COO})_2 \cdot 2\text{H}_2\text{O}$) were used as a source of copper (Cu) and nickel (Ni). In this synthesis procedure,

0.25 vol% of polyvinyl alcohol (PVA) was mixed with 250 ml double-deionized water and continuously stirred at 60 °C at 1000 rpm until it fully dissolves. After complete dissolution of PVA, the solution was kept and wait until it came to room temperature. During this time, the calculated amount ($\text{Ni}_{1-x}\text{Cu}_x\text{O}$, where $x = 0.001$) of 200 ml Nickel acetate tetra-hydrate ($\text{C}_4\text{H}_6\text{NiO}_4 \cdot 4\text{H}_2\text{O}$) and 200 ml Copper acetate di-hydrate ($\text{Cu}(\text{CH}_3\text{COO})_2 \cdot 2\text{H}_2\text{O}$) aqueous solution were prepared using double-deionized water. Finally, these two aqueous solutions were added with PVA solution at room temperature under continuous magnetic stirring. Thereafter, drop wise required amount of potassium hydroxide solution (KOH) was added to the mixture to bring the pH at 10. The resulting solution was kept in an air-tight container under constant magnetic stirring at 600 rpm for proper reaction and crystallization. The precipitated solution was centrifuged with a speed 12,000 rpm for 20 min. The obtained light green sample (0.1% Cu doped NiO) was then washed properly and dried in a vacuum oven at 80 °C for 36 h to evaporate the remaining part of water. Finally, an agate mortar was used to get free flowing light green powder sample. The as obtained sample was then annealed at 350 °C in a muffle furnace of temperature increment rate 5 °C/minute and holding time for two hours. The sample was acronym as CNO1 (350).

To synthesize the CNO/PVDF nanocomposite films, we initiated the process by dissolving PVDF pellets within a solution of DMF (Dimethyl formamide). This solution was homogeneously stirred for one hour at a temperature of 70 °C. Within this time, the PVDF pellets were completely dissolved in the DMF, resulting in a thick, transparent gel. Subsequently, we introduced the necessary weight percentages (20%, 25% and 30%) of CNO1 (350) nanoparticles into the PVDF gel. To achieve a uniform distribution of these nanoparticles within the polymer, we employed ultrasonication for a duration of two hours. The next step involved casting the homogeneous mixture of CNO/PVDF onto a glass plate to form the nanocomposite films. These glass plates were then placed onto a hot plate, where the solvent was gradually evaporated at 60 °C. We repeated the same procedure

to prepare a pure PVDF film for comparison. To ensure the consistency and accuracy, we measured the thickness of both the pure PVDF (PCNO 0) film and the PVDF nanocomposite (PCNO 20, PCNO 25, and PCNO 30) films loaded with CNO1 (350) nanoparticles. The precise measurements of these film thickness, along with detailed sample specifications, are provided in Table 1 for reference.

Characterization techniques

The X-ray diffraction (XRD) patterns of pure and nanocomposite films were acquired using a powder X-ray diffractometer (BRUKER AXS, Model D8, WI USA). The data were obtained using Cu K_α radiation ($\lambda = 1.5405 \text{ \AA}$) in the range of 2θ values covered was from 10° to 60° with scanning rate 0.3s/step. A field emission scanning electron microscope (FESEM) model INSECT F50 from FEI in the Netherlands was employed for morphological investigations at various magnifications, Energy dispersive X-ray (EDX) spectrum was used for elemental composition and elemental mapping. Fourier transform infrared (FTIR) measurements were conducted using a Spectrum 100 IR affinity instrument (PerkinElmer, Germany). To determine the zeta potential of CNO1 (350) nanoparticles, measurements were performed at room temperature with a Zetasizer Nano ZS (Malvern Instruments, UK). Dielectric properties (ϵ'), tangent loss ($\tan\delta$), and ac conductivity (σ_{ac}) were examined using an Agilent 4294 A Precision Impedance Analyzer at room temperature to investigate the electrical conduction mechanism of nanocomposite films.

Results and discussion

Mechanism of CNO-PVDF composite film formation

The present study delves into the investigation of the interaction mechanism between CNO1 (350) nano-fillers and the PVDF matrix, shedding light on the formation of CNO/PVDF interfaces as illustrated in Fig. 1. As demonstrated

Table 1

Sample Name	Sample Specification	Film Thickness (m)
PCNO 0	Pure PVDF film	4.3×10^{-2}
PCNO 20	20 wt% CNO1 (350) loaded PVDF film	3.9×10^{-2}
PCNO 25	25 wt% CNO1 (350) loaded PVDF film	4.2×10^{-2}
PCNO 30	30 wt% CNO1 (350) loaded PVDF film	3.6×10^{-2}

in Fig. 2(a), CNO1 (350) nanoparticles exhibited a negative zeta potential. This negative zeta potential signified an overall negative charge present in the CNO1 (350) nanofillers that were immersed within the Polymer (PVDF) gel. Through the application of solution casting, the closed-chain structure of PVDF, which corresponded to its α -phase, became accessible, exposing the all-trans planar zig-zag (TTTT) conformation feature of the β -phase of PVDF.

With a space group of Fd3m, the composition of CNO1 (350) was classified as a transition metal oxide of cubic rock-salt nanocrystalline system. The divalent metal cations Cu^{2+} substituted in the Ni^{2+} sites of NiO rock-salt assembly in the CNO1 (350) structure [39]. Five distinct crystalline phases, namely, α , β , γ , δ and ϵ phases [10, 23, 40, 55–60], are known to occur in PVDF. The all-trans planar zig-zag conformation of the β -phase produced a strong dipole moment because all of the electric dipoles aligning in a single direction.

Due to the electrostatic bonding, the interfaces between CNO1 (350) nanofillers and the PVDF matrix developed [18–20, 24, 61–63]. This was driven by the positive surface charge of the CH_2 groups in the PVDF matrix and the negative surface charge of CNO1 (350) nanofillers, as indicated by their negative zeta potential [64–66]. The CNO/PVDF nanocomposite films' overall polarity and polarization impact were amplified by the electrostatic interaction.

XRD analysis

The X-Ray diffraction (XRD) patterns of the studied samples, namely pure PVDF film (PCNO 0), and CNO1 (350) nanoparticle-loaded PVDF nanocomposite films (PCNO 20, PCNO 25 and PCNO 30), have been extensively examined and represented in Fig. 3(a). These patterns offered critical insights into the crystallographic properties and structural composition of the materials. It was noteworthy that all peaks in the patterns have been systematically assigned utilizing the JCPDS database. Specifically, the peaks in the XRD pattern of the pure PVDF sample (JCPDS card no. 10–0325) [54, 61], and the PCNO nanocomposite samples were meticulously matched to relevant phases [39, 45]. The non-appearance of impurity peaks underscores the exceptional purity and phase integrity of the films under scrutiny. The outline of XRD pattern of pure PVDF demonstrated peaks at different 2θ angles corresponded precisely with the non-polar α phase, γ phase, and polar β -phase of PVDF. These peaks validate the distinct crystalline phases present in the pure PVDF film.

Conversely, the peak positions in the XRD patterns of the CNO1 (350) nano-filler loaded PCNO nanocomposite samples exhibited subtle shifts with increasing loading percentages of nanoparticles in the polymer matrix. The emergence of internal lattice strain within the PVDF matrix was

Fig. 1 Schematic illustration of the mechanism of CNO1 (350)-PVDF composite film formation by solution casting approach

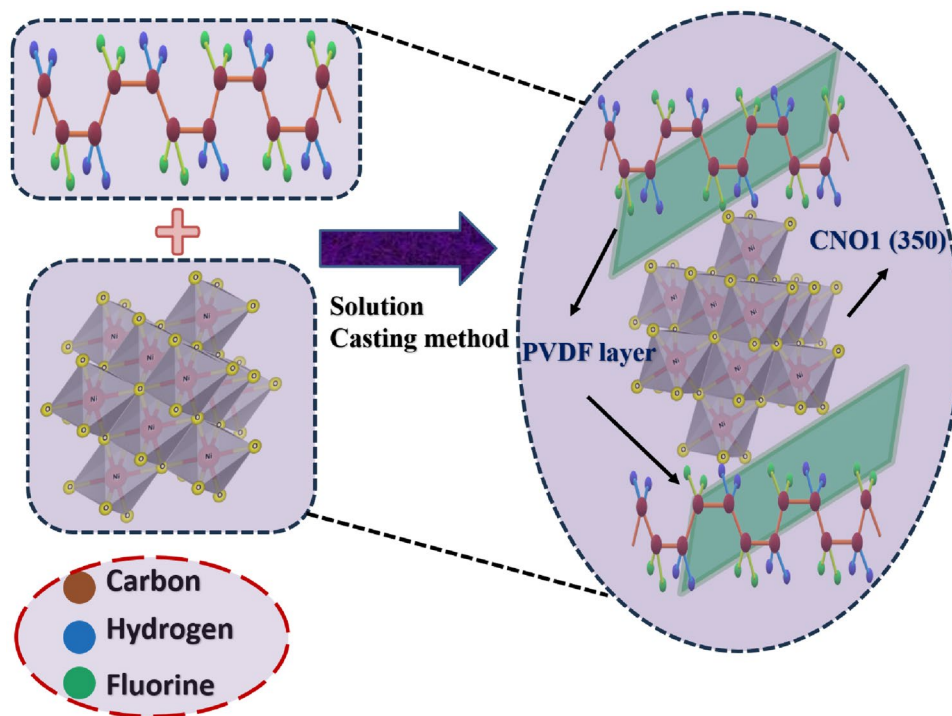
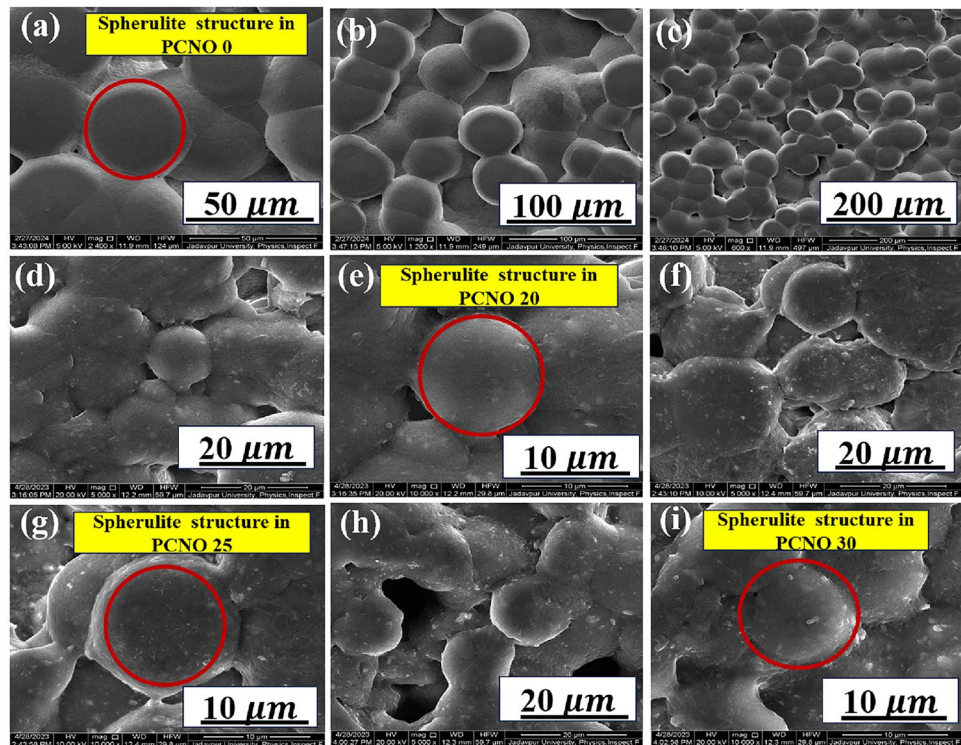


Fig. 2 a Graphical representation of zeta potential and its value for the sample CNO1 (350) **b** Schematic diagram of Probable β -Phase enhancement Mechanism of CNO-PVDF composite



indicated by this occurrence, suggesting the successful integration of the nanofiller. To further discern the presence of phase crystallization in the nanocomposite sample, attention was directed towards the differences in relative intensities of the (311) peak, specifically situated around 36° . The observed variation in the peak intensity was attributed to the alternations in phase crystallization within the PCNO nanocomposite samples. This phenomenon underscores the successful integration of CNO1 (350) nanoparticles into the PVDF matrix. This integration led to intriguing electrostatic interactions, as elaborated in forthcoming discussions. These interactions were characterized by the negatively charged surface of CNO1 (350) nanoparticles engaging with the positively charged hydrogen ligands within the PVDF host matrix [18–20, 24, 61–63].

FTIR analysis

FTIR Spectroscopy was employed to investigate how nanoparticles affect the electroactive β -crystalline phases within the PVDF. The obtained spectra, as shown in Fig. 3(b), revealed distinct vibrational bands that were associated with different phases. Specifically, vibrational bands at 763, 1149, and 1214 cm^{-1} were attributed to the α -phase [29, 30, 67] of the pristine PVDF. On the other hand, bands observed at 850 and 1277 cm^{-1} were indicative of the β -phase [29, 30, 67–69], while the peaks at 1232 cm^{-1} corresponded to the γ -phase [56].

From the analysis of Fig. 3(b), a notable observation was that the intensity of the α -phase bands decreased, while the peak at 850 cm^{-1} , corresponding to the β -phase, increased in intensity, with the progressive addition of CNO1 (350) nanoparticles. This phenomenon implied that the CNO1 (350) nanoparticles were present and enhanced the β -phase development within the PVDF matrix. This enhancement was primarily ascribed to the interfacial interaction that occurred between the CNO1 (350) nanoparticles and the PVDF matrix.

Furthermore, as the weight% of the filler increased, the appearance of the γ -phase became evident. This indicated the possibility of nucleation of the filler particles, as was also supported by evidence from XRD analysis.

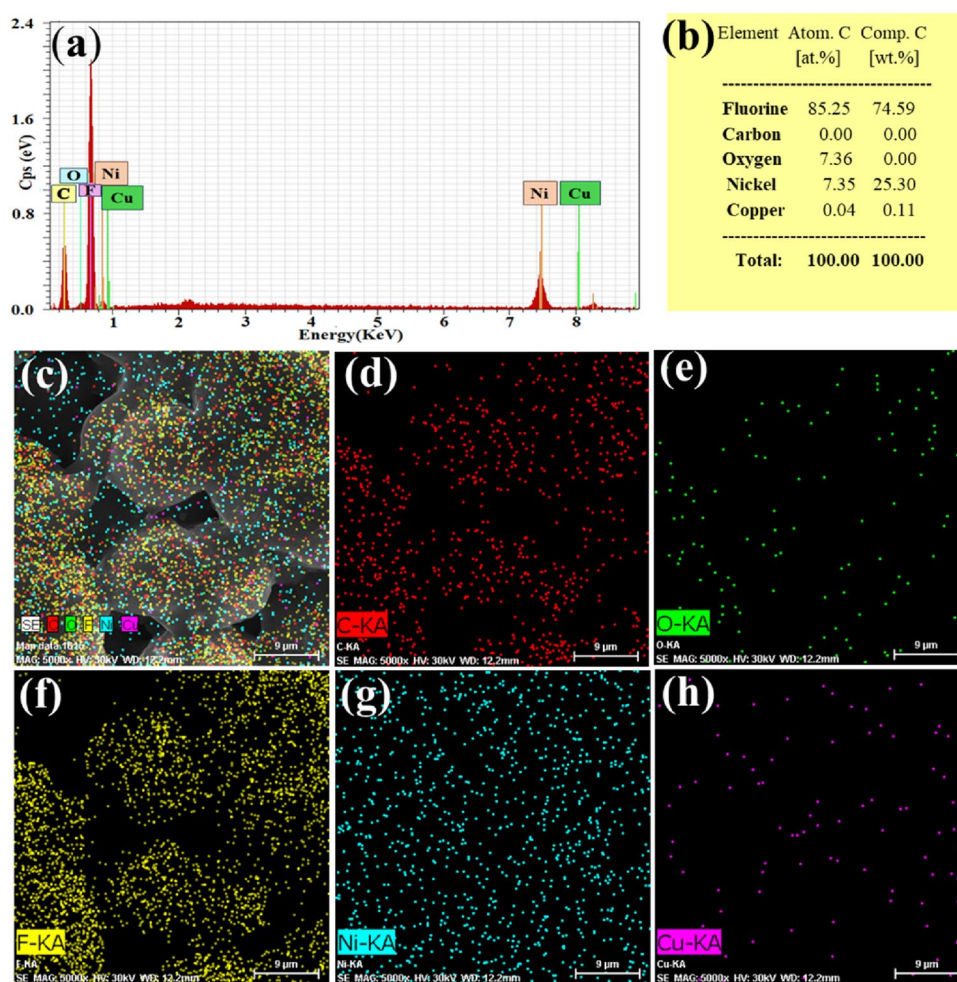
To quantify the relative fraction of the β -phase, the researcher utilized the Beer-Lambert law [40], which involved calculating the absorbance values at specific wavenumbers (763 cm^{-1} for α -phase and 850 cm^{-1} for β -phase):

$$F(\beta) = \frac{A(\beta)}{1.26A(\alpha) + A(\beta)}$$

where, $A(\beta)$ and $A(\alpha)$ corresponds to the absorbance at 850 cm^{-1} and 763 cm^{-1} respectively.

This calculation provided insights into the proportion of the β -phase present. The findings were visually represented through a diagram in Fig. 3(c). This diagram illustrated a

Fig. 3 **a** XRD patterns **b** FTIR spectra analysis **c** β -phase enhancement with sample concentration of our prepared samples and **d** Schematic representation of the enhancement in β - phase fraction of sample PCNO 25



gradual increase in the β -phase fraction as the filler loading increased up to 25 wt % of CNO1 (350). Specifically, in the 25 wt % CNO1 (350)-loaded PVDF composite film (referred to as PCNO 25), the number of aligned chains exhibiting an all-transplanar zig-zag (TTTT) conformation was effectively increased. Consequently, the enhancement resulted in a successful rise of the β -phase fraction to 68.2%, compared to the 38.9% observed in the unmodified PVDF [Fig. 3(c)].

However, as the concentration of CNO1 (350) nanofillers within the PVDF matrix was further increased, the β -phase percentage was diminished. This phenomenon was particularly evident in the case of PCNO 30, where the β -phase percentage drops to 55%. This reduction was attributed to the constrained movement of polymer chains in all transplanar zig-zag (TTTT) conformation when higher nanofiller loading percentages made the agglomeration effect more pronounced. Consequently, this constraint limited the crystallization of the β -phase within the composite system. Figure 3(d) represents a schematic diagram of β -phase enhancement of 25 wt% CNO1 (350) doped PVDF sample (PCNO 25).

The following explanation explained the all-transplanar zig-zag (TTTT) conformation, and the amplification of the polar β -phase in all CNO/PVDF composite films when compared to PCNO 0 (PVDF without fillers).

In Fig. 2(a), a negative zeta potential of around -8.23 mV was depicted for CNO1 (350) nanoparticles [70]. This negative zeta potential indicated the presence of a negative charge across the surface of the nanoparticles when they were immersed within the PVDF gel. In context of FTIR absorption spectra, it was revealed that compared to pure PVDF (referred to as PCNO 0), the β -phase percentage in CNO -PVDF composite films were enhanced which can be attributed to the ion-dipole interaction between the surface charge of CNO1 (350) and the positively charged $-\text{CH}_2$ -dipoles of PVDF in the nanocomposite films [18–20, 24, 56, 61–63, 71]. This interaction enhanced the polarization effect within the PVDF matrix, supported by the electroactive characteristics of the CNO1 (350) nanoparticles. This augmentation made these composite films progressively more polarized and electroactive compared to the pure PVDF (PCNO 0) [18–20, 24, 56, 61–63, 71].

FESEM analysis

Figure 4(a-i) represented the FESEM micrographs, offering crucial insights into the enhanced β -phase crystallization of PVDF host material through structural morphology variations in CNO/PVDF nanocomposite films [61, 72–74]. Red circle showing the spherulite structure of PVDF spherulite structures. The observed surface morphologies of both pure PVDF and CNO1 (350) nanoparticle decorated PVDF nanocomposite membranes were detailed in this section, using representative micrographs to distinctly highlight the differences.

As indicated in our previous study, the microstructure of CNO1 (350) nanoparticles appeared mostly non-spherical agglomerated morphology with consistent size exhibiting micropores and larger specific surface areas [39] which is consistent with both FESEM observations and XRD analysis results.

The surface morphology of pure PVDF film (in our case PCNO 0) exhibited a combination of spherulite and radial lamellar structures as presented in previous literatures [18–20, 24]. The presence of spherulites confirmed the existence of the polar β -phase, while the lamellae indicated the non-polar α -phase. Hence, the PCNO film displayed a mixture of α and β -phases but with a slightly greater presence of the β -phase.

A distinct contrast in surface morphology between pure PVDF and CNO1 (350) incorporated PVDF was evident from the micrographs in Fig. 4(a-i). The crystalline phases in PVDF were known to change with the modification of synthesis methods and nanofiller content. The incorporation of CNO1 (350) nanofiller led to a more pronounced presence of the polar β -phase, primarily in the form of bubble-like spherulites.

As nucleation centers in the PVDF matrix, CNO1 (350) nanoparticles promoted the transition from the α -phase to the electroactive β -phase. This transformation was evidenced

by the prevalence of bubble-like spherulite structures on the surface of PCNO 0, PCNO 20, PCNO 25 and PCNO 30 films [19, 20, 61–63, 75]. The role of CNO1 (350) nanofillers was crucial in promoting the alignment of molecular dipoles, resulting in enhanced crystallization of the polar β -phase. The presence of bubble-like spherulite structures across the film surface signified the enhanced β -phase crystallization due to the CNO1 (350) nanofillers. The details regarding the variations in phase crystallization in PCNO 0, PCNO 20, PCNO 25, and PCNO 30 films were also discussed in the FTIR section. As a result, this significant improvement validated the potential of PCNO nanocomposite materials for diverse applications in the field of dielectric, capacitive and energy storage devices etc.

EDX and elemental mapping analysis

The EDX analysis and corresponding elemental area mapping of sample PCNO 25 were represented in Fig. 5(a-h), respectively. These findings definitively confirmed the presence of Copper (Cu), Nickel (Ni), and Oxygen (O) ions within the PCNO 25 nanocomposite film, which corresponded to the CNO1 (350) nanofillers used in the CNO/PVDF composite materials. The Carbon (C) peak in the EDX analysis might arise due to the use of carbon tape during FESEM observation or due to the PVDF polymer. The presence of Fluorine (F) due to utilization of PVDF was also verified from the EDX spectrum and elemental mapping. No peak corresponding to Hydrogen (H) was recorded due to the limitation of EDX and elemental mapping. Furthermore, the elemental area mapping of the PCNO 25 composite film exhibited a nearly uniform distribution of all the ions including Nickel (Ni), Copper (Cu), and Oxygen (O), within the composite film.

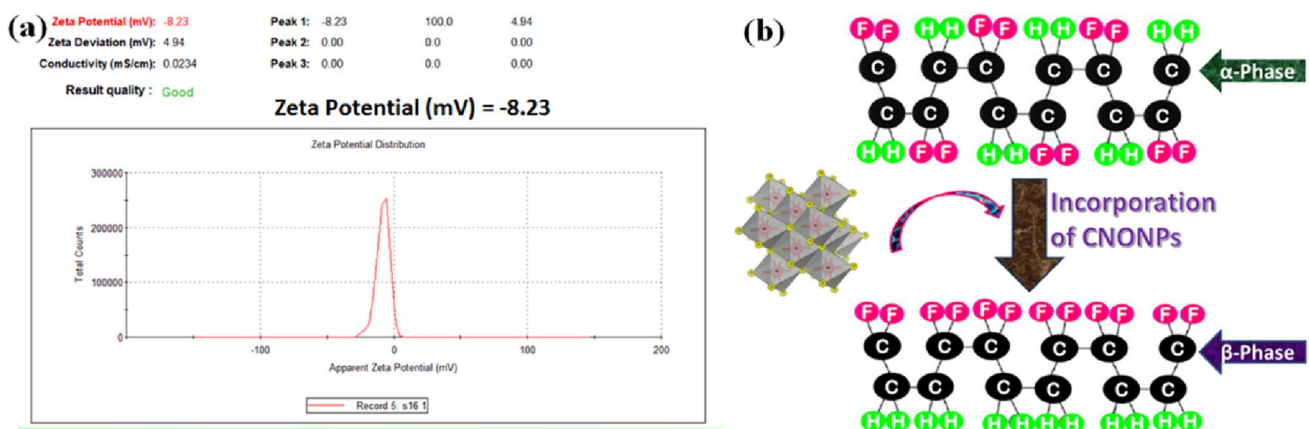
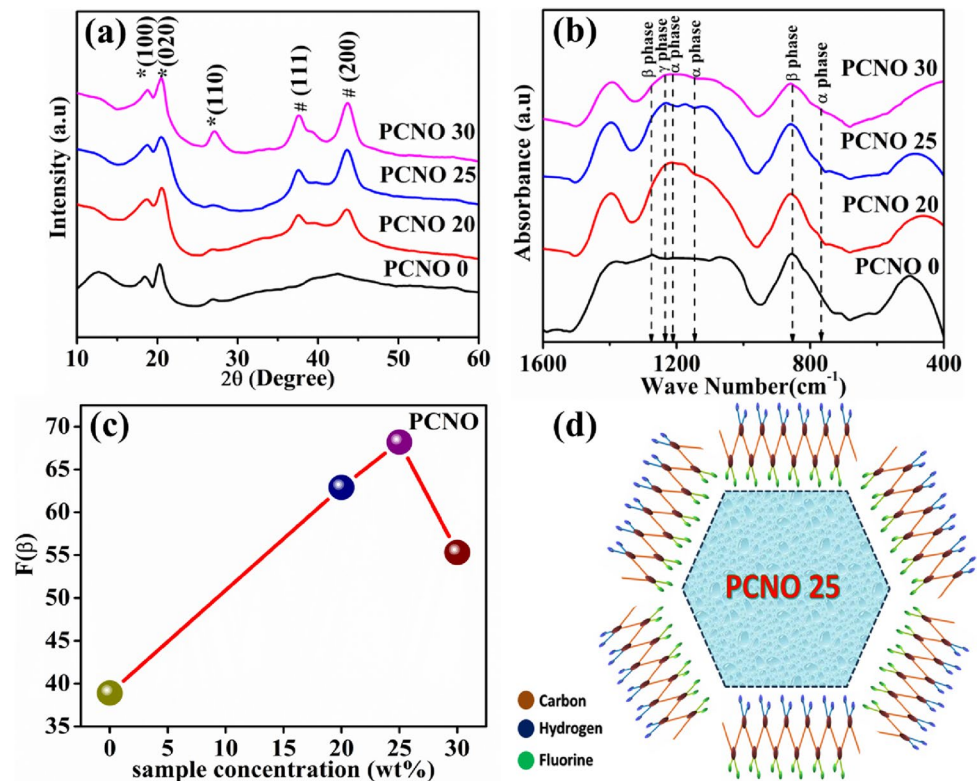


Fig. 4 FESEM micrograph of our prepared sample at various magnifications: **a**, **b** PCNO 20; **c**, **d** PCNO 25; and **e**, **f** PCNO 30

Fig. 5 **a** Energy Dispersive X-ray (EDX) micrograph **b** Corresponding percentage of elemental composition and **c** - **h** Elemental area mapping for sample PCNO 25.



Probable β -Phase enhancement mechanism

The XRD, FTIR, and morphological analyses of the nanocomposite films validate the introduction of 0.1% copper doped nickel oxide nanoparticles [CNO1 (350)] into the PVDF matrix, prompting a notable increase in the electroactive β -phase formation. Unlike neat PVDF films, which predominantly contain the α -phase, the incorporation of CNO1 (350) promotes the transformation of PVDF into the electroactive β -polymorph. This transformation results from both the inclusion and uniform dispersion of CNO1 (350) within the PVDF matrix.

The interaction occurring between copper doped nickel oxide nanoparticles and the polymer matrix is an important topic to investigate here since it actively facilitates the formation of the electroactive β -phase. Strong interactions between the implanted nanoparticles and the PVDF matrix are primarily responsible for the significant enhancement of the electroactive β -phase fraction. One driving force for this transformation is the ion-dipole interaction occurring between the PVDF matrix and the copper doped nickel oxide nanoparticles. Figure 2(a) displays the graph depicting CNO1 (350) nanoparticles with a negative zeta potential, of approximately -8.23 mV. This negative zeta potential plays a crucial role in enhancing the electroactive β -phase fraction of CNO/PVDF nanocomposite films compared to pure PVDF (PCNO 0) films. Previous

research has indicated such interactions, as PVDF chains with partially positive $-\text{CH}_2$ dipoles exhibit strong electrostatic attractions with the negatively charged nanoparticle surfaces [56, 71]. This interaction leads to the alignment of PVDF chains on the nanoparticle surfaces in an extended all-trans (TTT) conformation, ultimately forming the electroactive β -phase. The nanoparticles' surfaces serve as nucleation sites for the β -phase formation. The electroactive β -phase formation process is explained by the schematic diagram in Fig. 2(b), which illustrates the ion-dipole interaction mechanism between the nanoparticles and polymer chains. It is noteworthy that our finding indicates the presence of a minor amount of the electroactive γ -phase in the loaded PVDF films. This occurrence may be linked to the gauge effect, potentially emerging from local internal chain rotations.

Thermal properties analysis

Figure 6 shows the DSC thermograph of pure PVDF and CNO1 (350) nanoparticles-loaded PVDF composite films. The melting peak at 170.06 °C in the pure PVDF thermograph corresponds to the nonpolar α polymorph of PVDF [21, 53]. This phenomenon suggests a morphological change in the crystallinity of PVDF, specifically the transition from nonpolar α crystal morph (TGTG conformation) to β crystal morph (TTTT conformation). In good conformity with XRD results,

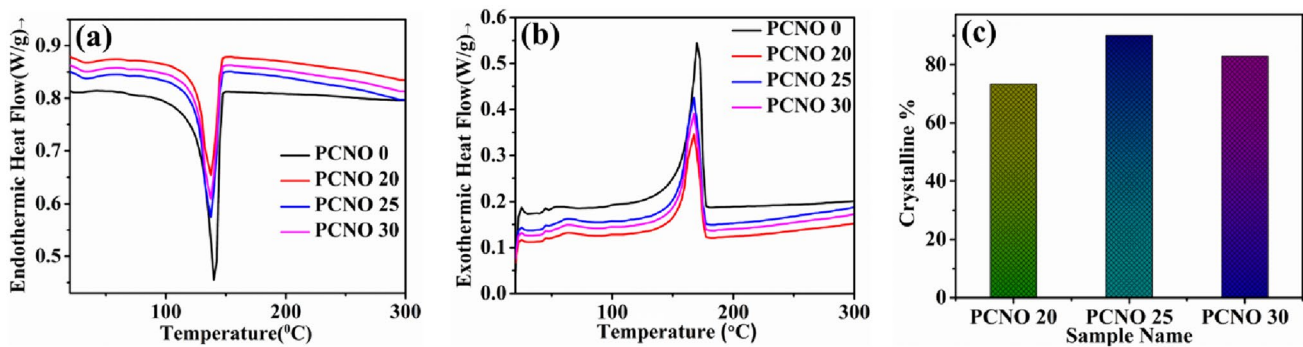


Fig. 6 a, b DSC thermograph of pure PVDF and CNO1 (350) nanoparticles-loaded PVDF composite films and c Diagram of change in crystalline % of CNO1 (350) nanoparticles-loaded PVDF composite films

this change occurs. The melting temperature (T_c) changes with the loading of CNO1 (350) NPs. The CNO1 (350) NPs play an important role as a nucleating agent for PVDF, as suggested by this result. Equation (1) [21, 46, 76] was used to quantitatively measure the degree of crystallinity (X_c).

$$\text{Crystallinity \%} = \frac{\Delta H_m}{\Delta H^0} \times 100 \quad (1)$$

The symbol ΔH_m represents the melting enthalpy or enthalpy of fusion, while ΔH^0 denotes the melting enthalpy of pure PVDF. In Fig. 6(b) and (c), the enthalpy of fusion (ΔH_m) and the degree of crystallinity (X_c) of both pure and composite PVDF films are depicted. Figure 6(c) illustrates that the enthalpy of fusion and the degree of crystallinity (X_c) increase up to a loading of 25 wt % of CNO1 (350) NPs in the PVDF matrix, after which they decrease with further loading of the CNO1 (350) NPs. The maximum degree of crystallinity (X_c) achieved was 90.04% for PCNO 25.

Electrical properties analysis

The assessment of frequency-dependent dielectric response stands as a pivotal metric in comprehending the characteristics of CNO/PVDF nanocomposite films, especially in their potential applications for energy storage and electromagnetic interference (EMI) shielding applications. This response is encapsulated in the real part of the dielectric constant (ϵ'), a parameter calculated using the formula,

$$\epsilon' = \frac{C \cdot d}{\epsilon_0 A} \quad (2)$$

[31, 44, 47, 53, 77–80] and

$$\epsilon'' = \epsilon' \times \tan \delta \quad (3)$$

[44, 53, 78–80] where C represents the capacitance of the sample, d and A denote thickness and cross-sectional area of the pellet, and ϵ_0 symbolizes the free space permittivity. Notably, the figures in our study, Fig. 7(a) and (d), offer

a compelling visual narrative. They illustrate a gradual increase in the real part of the dielectric constant (ϵ') from PCNO 0 to PCNO 25, with PCNO 25 exhibiting the highest value ($\epsilon' \sim 63$). The underlying mechanisms behind this phenomenon are two-fold:

Firstly, the incorporation of CNO1 (350) nanoparticles in PVDF leads to an increase in the β -phase crystallization, which corresponds to an increase in ϵ' . This is evident from the FTIR spectra, where the β -phase fraction ($F(\beta)\%$) peaks at PCNO 25.

Secondly, the Maxwell-Wagner-Sillars interfacial polarization effect [44, 48, 81] comes into play in heterogeneous media, like these nanocomposite films, causing the accumulation of free charges at interfaces. The number of effective interfaces increases with higher CNO1 (350) nanoparticle loading, optimizing at 25 wt% (PCNO 25). However, beyond this threshold value 25 wt% (PCNO 25), excessive nanoparticles lead to agglomeration, reducing effective interfaces and subsequently decreasing the overall dielectric performance. Furthermore, our observations reveal that the dielectric response experiences a decrease (~ 60 to ~ 42 for PCNO 25 sample) with an increasing frequency (40 Hz to 1 MHz) at room temperature (RT). This decrement tendency is attributed to electrons lagging behind the alternating electric field beyond a certain critical frequency. In Fig. 7(b) and (e), it is observed that the dielectric loss decreases from ~ 10 to 0.09 for PCNO 25 sample with increasing frequency up to 20 kHz at room temperature, primarily because of the space charge polarization. The higher CNO1 (350) nanoparticle content is primarily responsible for increasing $\tan \delta$ due to the formation of conducting pathways between the nanoparticles in comparison to PVDF. For further increment of the frequency after 10 kHz the dielectric loss increases from ~ 0.1 at 10 kHz to 0.3 at 1 MHz because of the dissipation of energy due to the externally applied electric field within the composite matrix further contributing to the escalation of $\tan \delta$. In direct comparison to pure PVDF (PCNO 0), the CNO/PVDF nanocomposite films manifest a more pronounced frequency dependence within the lower frequency range (below 10 kHz). Moreover, the heightened frequency

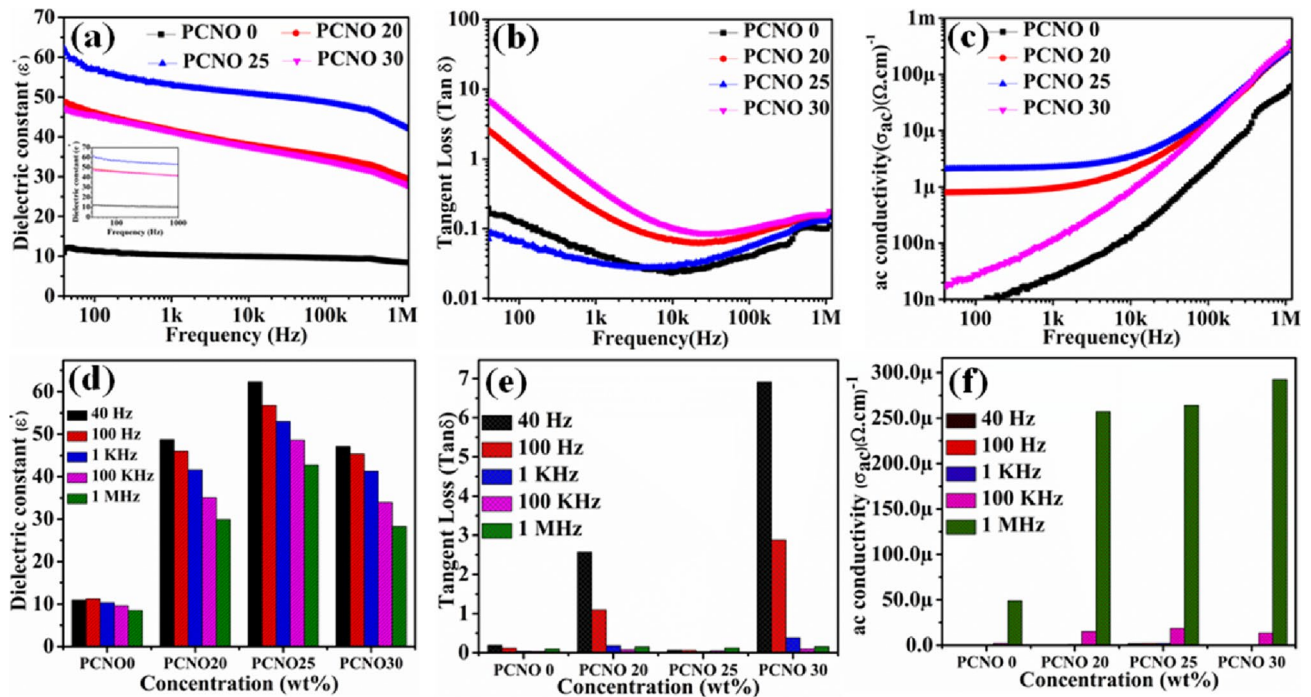


Fig. 7 Plots of **a** Dielectric constant **b** Loss tangent and **c** ac conductivity at room temperature, with varied frequencies (40 Hz–1 MHz) of prepared samples. The plots of **d** dielectric constant **e** tangent loss

and **f** ac conductivity at different frequencies (40 Hz, 100 Hz, 1 kHz, 100 kHz, and 1 MHz) at room temperature of prepared samples

dependence observed in the composite is attributed to the unique polarization mechanisms intrinsic to CNO1 (350) nanoparticles. These mechanisms involve the rapid reorientation of dipoles within the nanoparticles in response to the alternating electric field, leading to increased losses (~ 0.1 at 10 kHz to 0.3 at 1 MHz) at higher frequencies. However, as the frequency surpasses 10 kHz, a shift occurs in the dominant relaxation mechanism within the composite. At this point, the relaxation mechanism within the frequency range 10 kHz to 100 kHz associated with the β -phase of PVDF becomes more prominent, exerting a greater influence on the overall dielectric behavior of the material. This transition suggests a dynamic interplay between the polarisation mechanisms of CNO1 (350) nanoparticles and the intrinsic properties of PVDF, ultimately shaping the composite's response to varying frequencies from 40 Hz to 1 MHz. Understanding this frequency-dependent behavior is crucial for optimizing the performance of the composite in specific applications requiring tailored dielectric properties across different frequency ranges. Rather than Maxwell-Wagner-Sillars interfacial polarization as observed at lower frequencies, the dielectric loss tangent of the CNO/PVDF nanocomposite films in the higher frequency range (above 100 kHz) aligns well with the loss tangent behavior seen in the pure PVDF (PCNO 0) system. Figure 7(c) and (f) depict the assessment of the electrical conduction mechanism through ac conductivity measurements. Prior studies have consistently

emphasized the trend of increasing ac conductivity ($2 \mu\Omega \text{ cm}^{-1}$ to $500 \mu\Omega \text{ cm}^{-1}$) with the frequency of the applied alternating electric field in nano-filler loaded PVDF nanocomposites. This phenomenon is typically attributed to the heightened migration of induced free charge carriers across grain boundaries within the composite structure. However, our research findings, as illustrated in Fig. 7(c), unveil a compelling departure from this conventional expectation. Surprisingly, the ac conductivity observed across all nanocomposite samples demonstrates complete independence

Table 2 A comparative study of dielectric constant of CNO1 (350) nanoparticles incorporated PVDF film with some commercially available and previously reported polymer-based separators

Sl no	Materials	Dielectric constant	Reference
1	ZnO/PVDF	13.01	[82]
2	Ca doped ZnO/PVDF	15	[83]
3	Fe doped ZnO/PVDF-TrFE	21.03	[84]
4	MgO/PVDF	35	[49]
5	BaTiO ₃ /NiO/PVDF	24	[54]
6	Li ³⁺ irradiated PVDF	6.8	[54]
7	Li ³⁺ irradiated (0.8) PVDF/ (0.2) BaTiO ₃	10.7	[50]
8	PVDF/PPG/LiCl+ SrTiO ₃	4.3	[25]
9	This work	63	

from the frequency of the applied electric field, challenging the established understanding of electrical conduction in such materials. This unexpected behavior suggests the presence of unique conduction pathways or mechanisms within our composite system, warranting further investigation to unravel the underlying principles governing its electrical properties Table 2.

Conclusion

PVDF composite films were prepared using the solution casting method and filled with CNO1 (350) nanoflakes synthesized through a modified chemical synthesis approach. The results from X-ray diffraction and FT-IR analyses reveal that the inclusion of CNO1 (350) filler promotes the organization of crystalline chains within the polymer matrix, inducing the growth of polymorphic β -phase crystallites through heterogeneous nucleation. FESEM results demonstrate the agglomeration of CNO1 (350) nanoflakes as hierarchical-like structures within the polymer matrix, albeit with a homogeneous dispersion. In accordance with percolation theory, the conductivity of the composite films is influenced by interparticle spacing and CNO1 (350) filler content, with a percolation threshold identified at approximately 25 wt%. The obtained dielectric constant in our samples is more than six times larger than that of the bare PVDF film without a filler. A proposed explanation for this behavior attributes the improvement in dielectric properties to Maxwell–Wagner polarization as the primary mechanism. These findings suggest that CNO1 (350)/PVDF composite films hold potential for the production of electronic devices with enhanced dielectric and electrical characteristics, such as high charge-storage capacitors or flexible electronic devices.

Acknowledgements The first author wishes to thank the Department of Physics, Jadavpur University for the necessary infrastructural facilities. He also gratefully acknowledges the Department of Physics, Bangabasi College, University of Calcutta for their valuable support and necessary co-operation.

Data availability Data should be available on request.

Declarations

Conflict of interest The authors declare no conflict of interest.

References

- Sau S, Kundu M, Biswas S et al (2024) Tailoring ZnMnO₃ nanostructures: a promising strategy for high energy density asymmetric supercapacitors. *J Energy Storage* 85:111069. <https://doi.org/10.1016/j.est.2024.111069>
- Kundu M, Mondal D, Mondal I et al (2023) A rational preparation strategy of phase tuned MoO₃ nanostructures for high-performance all-solid asymmetric supercapacitor. *J Energy Chem* 87:192–206. <https://doi.org/10.1016/j.jechem.2023.08.014>
- Chen T, Tang Q, Wang B et al (2015) Dielectric and magnetic properties of poly(vinylidene fluoride) composites doped with pomegranate-like PPY@NiFe₂O₄ nanospheres. *Mater Lett* 159:413–416. <https://doi.org/10.1016/j.matlet.2015.07.050>
- Du Pasquier A, Warren PC, Culver D et al (2000) Plastic PVDF-HFP electrolyte laminates prepared by a phase-inversion process. *Solid State Ionics* 135:249–257. [https://doi.org/10.1016/S0167-2738\(00\)00371-4](https://doi.org/10.1016/S0167-2738(00)00371-4)
- Johnsi M, Suthanthiraraj SA (2016) Compositional effect of ZrO₂ nanofillers on a PVDF-co-HFP based Polymer electrolyte system for solid state zinc batteries. *Chin J Polym Sci (English Ed)* 34:332–343. <https://doi.org/10.1007/s10118-016-1750-3>
- Henderson WA, Brooks NR, Young VG (2003) Single-crystal structures of polymer electrolytes. *J Am Chem Soc* 125:12098–12099. <https://doi.org/10.1021/ja036535k>
- Page SEEL (2006) A dielectric polymer with. *Synthesis (Stuttg)* 313:2–5
- Li N, Huang Y, Du F et al (2006) <Nano letters 6 issue 6 2006 [doi 10.102.pdf>. *Nano Lett* 6:1–5
- Twinkle, Kaur M, Gowsamy JK et al (2020) Synthesis and characterization of CNT/PVDF paper for electronic and energy storage applications. *Emergent Mater* 3:181–185. <https://doi.org/10.1007/s42247-020-00074-5>
- Saxena P, Shukla P (2021) A comprehensive review on fundamental properties and applications of poly(vinylidene fluoride) (PVDF). *Adv Compos Hybrid Mater* 4:8–26. <https://doi.org/10.1007/s42114-021-00217-0>
- Zhou W, Chen Q, Sui X et al (2015) Enhanced thermal conductivity and dielectric properties of Al/ β -SiCw/PVDF composites. *Compos Part Appl Sci Manuf* 71:184–191. <https://doi.org/10.1016/j.compositesa.2015.01.024>
- Zirkel M, Sawatdee A, Helbig U, Krause M, Scheipl G, Kraker E, Ersman PA, Nilsson D, Platt D, Bodö P, Bauer S, Domann G, Stadlober B (2011) An All-Printed Ferroelectric Active Matrix Sensor Network Based on Only Five Functional Materials Forming a Touchless Control Interface. *Adv. Mater.* 23:2069–2074. <https://doi.org/10.1002/adma.201100054>
- Wu G, Cheng Y, Wang Z et al (2017) In situ polymerization of modified graphene/polyimide composite with improved mechanical and thermal properties. *J Mater Sci Mater Electron* 28:576–581. <https://doi.org/10.1007/s10854-016-5560-8>
- Yu J, Huang X, Wu C et al (2012) Interfacial modification of boron nitride nanoplatelets for epoxy composites with improved thermal properties. *Polym (Guildf)* 53:471–480. <https://doi.org/10.1016/j.polymer.2011.12.040>
- Aliane A, Benwadih M, Bouthinon B et al (2015) Impact of crystallization on ferro-, piezo- and pyro-electric characteristics in thin film P(VDF-TrFE). *Org Electron* 25:92–98. <https://doi.org/10.1016/j.orgel.2015.06.007>
- Li ZM, Li L, Bin, Shen KZ et al (2004) In-situ microfibrillar PET/iPP blend via slit die extrusion, hot stretching, and quenching: influence of hot stretch ratio on morphology, crystallization, and crystal structure of iPP at a fixed PET concentration. *J Polym Sci Part B Polym Phys* 42:4095–4106. <https://doi.org/10.1002/polb.20262>
- Zhang Z, Cui S, Ma R et al (2023) Melt stretching and quenching produce low-crystalline biodegradable poly(lactic acid) filled with β -form shish for highly improved mechanical toughness. *Int J Biol Macromol* 251:126220. <https://doi.org/10.1016/j.ijbiomac.2023.126220>
- Chakraborty T, Sharma S, Debnath T et al (2021) Fabrication of heterostructure composites of Ni-Zn-Cu-Ferrite-C₃N₄-Poly(vinylidene fluoride) films for the enhancement of electromagnetic interference

- shielding effectiveness. *Chem Eng J* 420:127683. <https://doi.org/10.1016/j.cej.2020.127683>
19. Chakraborty T, Dutta S, Mahapatra AS et al (2023) Superior EMI shielding effectiveness of light weight and stretchable X-type hexaferrite-poly(vinylidene fluoride) laminated nanocomposite materials. *J Magn Magn Mater* 570:170508. <https://doi.org/10.1016/j.jmmm.2023.170508>
 20. Saha S, Chakraborty T, Saha A et al (2024) A multi-layer design of hexaferrite decorated graphene derivatives incorporated PVDF nanocomposite films; understanding the role of GO/rGO for outstanding electromagnetic wave absorption at microwave frequencies. *Carbon N Y* 220:118829. <https://doi.org/10.1016/j.carbon.2024.118829>
 21. Mishra S, Sahoo R, Unnikrishnan L et al (2020) Effect of multi-step processing on the structural, morphological and dielectric behaviour of PVDF films. *Ionics (Kiel)* 26:6069–6081. <https://doi.org/10.1007/s11581-020-03770-8>
 22. Crespi F, Gavagnin G, Sánchez D, Martínez GS (2017) Supercritical carbon dioxide cycles for power generation: a review. *Appl Energy* 195:152–183. <https://doi.org/10.1016/j.apenergy.2017.02.048>
 23. Jayakumar OD, Abdelhamid EH, Kotari V et al (2015) Fabrication of flexible and self-standing inorganic-organic three phase magneto-dielectric PVDF based multiferroic nanocomposite films through a small loading of graphene oxide (GO) and Fe₃O₄ nanoparticles. *Dalt Trans* 44:15872–15881. <https://doi.org/10.1039/c5dt01509j>
 24. Saha P, Debnath T, Das S et al (2019) β -Phase improved Mn-Zn-Cu-ferrite-PVDF nanocomposite film: A metamaterial file:///E:/PhD File/Paper II (Film)/Communication Related documents/Journal of Polymer Research 19.12.23/Response to Reviewer/Reference/S. Sutrardhar1-s2.0-S0921510719301230-main.pdf f. *Mater Sci Eng B* 245:17–29. <https://doi.org/10.1016/j.mseb.2019.05.006>
 25. Alvarez-Sanchez CO, Lasalde-Ramirez JA, Ortiz-Quiles EO et al (2019) Polymer-MTiO₃ (M = Ca, Sr, Ba) composites as facile and scalable supercapacitor separators. *Energy Sci Eng* 7:730–740. <https://doi.org/10.1002/ese3.299>
 26. Paul BK, Roy D, Manna S et al (2018) High dielectric response of cobalt aluminate mullite (CAM) nanocomposite over cobalt aluminate mullite polymer (CAMP) nanocomposite in PVDF matrix. *J Electroceram* 40:347–359. <https://doi.org/10.1007/s10832-018-0136-z>
 27. Mondal A, Basu R, Das S, Nandy P (2011) Beneficial role of carbon nanotubes on mustard plant growth: an agricultural prospect. *J Nanoparticle Res* 13:4519–4528. <https://doi.org/10.1007/s11051-011-0406-z>
 28. Sarkar D, Bhattacharya A, Nandy P, Das S (2014) Enhanced broadband microwave reflection loss of carbon nanotube ensheathed Ni-Zn-Co-ferrite magnetic nanoparticles. *Mater Lett* 120:259–262. <https://doi.org/10.1016/j.matlet.2014.01.089>
 29. Yang Y, Li Z, Ji W et al (2018) Enhanced dielectric properties through using mixed fillers consisting of nano-barium titanate/nickel hydroxide for polyvinylidene fluoride based composites. *Compos Part Appl Sci Manuf* 104:24–31. <https://doi.org/10.1016/j.compositesa.2017.10.024>
 30. Dutta B, Kar E, Sen G et al (2020) Lightweight, flexible NiO@SiO₂/PVDF nanocomposite film for UV protection and EMI shielding application. *Mater Res Bull* 124:110746. <https://doi.org/10.1016/j.materresbull.2019.110746>
 31. Dutta B, Kar E, Bose N, Mukherjee S (2018) NiO@SiO₂/PVDF: a flexible polymer nanocomposite for a high performance human body motion-based Energy Harvester and Tactile e-Skin Mechanosensor. *ACS Sustain Chem Eng* 6:10505–10516. <https://doi.org/10.1021/acssuschemeng.8b01851>
 32. Roy D, Bagchi B, Das S, Nandy P (2013) Electrical and dielectric properties of sol-gel derived mullite doped with transition metals. *Mater Chem Phys* 138:375–383. <https://doi.org/10.1016/j.matchemphys.2012.11.070>
 33. Bhattacharya D, Ghoshal D, Mondal D et al (2019) Visible light driven degradation of brilliant green dye using titanium based ternary metal oxide photocatalyst. *Results Phys* 12:1850–1858. <https://doi.org/10.1016/j.rinp.2019.01.065>
 34. Mondal D, Paul BK, Bhattacharya D et al (2021) Copper-doped α -MnO₂ nano-sphere: metamaterial for enhanced supercapacitor and microwave shielding applications. *J Mater Chem C* 9:5132–5147. <https://doi.org/10.1039/d0tc06085b>
 35. Das S, Das S, Sutrardhar S (2017) Effect of Gd³⁺ and Al³⁺ on optical and dielectric properties of ZnO nanoparticle prepared by two-step hydrothermal method. *Ceram Int* 43:6932–6941. <https://doi.org/10.1016/j.ceramint.2017.02.116>
 36. Ibois L, Bernes A, Teyssedre G et al (2000) Correlation between pyroelectric properties and dielectric behaviour in ferroelectric polymers. *Ferroelectrics* 238:163–170. <https://doi.org/10.1080/00150190008008780>
 37. Xia W, Xu Z, Zhang Q et al (2012) Dependence of dielectric, ferroelectric, and piezoelectric properties on crystalline properties of p(VDF-co-TrFE) copolymers. *J Polym Sci Part B Polym Phys* 50:1271–1276. <https://doi.org/10.1002/polb.23125>
 38. Lovinger AJ (1983) Ferroelectric Transition in a Copolymer of Vinylidene Fluoride and Tetrafluoroethylene. *Macromolecules* 16:1529–1534. <https://doi.org/10.1021/ma00243a021>
 39. Biswas S, Saha Y, Mondal I et al (2023) Synergistic approach for enhancement of optical and electrical dielectric properties of size-tunable Cu doped NiO semiconductor quantum nanoflakes. *Curr Appl Phys* 56:66–78. <https://doi.org/10.1016/j.cap.2023.10.002>
 40. Thakur P, Kool A, Hoque NA et al (2018) Superior performances of in situ synthesized ZnO/PVDF thin film based self-poled piezoelectric nanogenerator and self-charged photo-power bank with high durability. *Nano Energy* 44:456–467. <https://doi.org/10.1016/j.nanoen.2017.11.065>
 41. Meng N, Zhu X, Mao R et al (2017) Nanoscale interfacial electroactivity in PVDF/PVDF-TrFE blended films with enhanced dielectric and ferroelectric properties. *J Mater Chem C* 5:3296–3305. <https://doi.org/10.1039/c7tc00162b>
 42. Sun GW, Jin MJ, Liu QY et al (2023) Unveiling the enhancement essence on Li₂S deposition by the polarized topological β -polyvinylidene fluoride: beyond built-in electric field effect. *Chem Eng J* 453:139752. <https://doi.org/10.1016/j.cej.2022.139752>
 43. Choi KH, Cho SJ, Kim SH et al (2014) Thin, deformable, and safety-reinforced plastic crystal polymer electrolytes for high-performance flexible lithium-ion batteries. *Adv Funct Mater* 24:44–52. <https://doi.org/10.1002/adfm.201301345>
 44. Praveen H, Chandran VG (2023) Effects of doping nickel oxide in dielectric property and electrical conductivity of poly (O-toluidine). *J Mater Sci Mater Electron* 34:1–10. <https://doi.org/10.1007/s10854-023-10884-y>
 45. Huang L, Wang Y, Zhu X et al (2021) Mg-Doped nickel oxide as efficient hole-transport layer for Perovskite Photodetectors. *J Phys Chem C* 125:16066–16074. <https://doi.org/10.1021/acs.jpcc.1c04888>
 46. Parangusan H, Ponnamma D, Almaadeed MAA (2018) Investigation on the effect of γ -irradiation on the dielectric and piezoelectric properties of stretchable PVDF/Fe-ZnO nanocomposites for self-powering devices. *Soft Matter* 14:8803–8813. <https://doi.org/10.1039/c8sm01655k>
 47. Mondal I, Saha Y, Halder P et al (2023) Synchronization of theoretical and experimental studies on the enriched optical and dielectric properties of size modulated CoCr₂O₄ quantum dots. *Solid State Sci* 146:107342. <https://doi.org/10.1016/j.solidstateciences.2023.107342>
 48. Mondal D, Das S, Paul BK et al (2019) Size engineered Cu-doped α -MnO₂ nanoparticles for exaggerated photocatalytic activity and energy storage application. *Mater Res Bull* 115:159–169. <https://doi.org/10.1016/j.materresbull.2019.03.023>

49. Rozana MD, Arshad AN, Wahid MH et al (2012) Dielectric constant of PVDF/MgO nanocomposites thin films. ISBEIA 2012 - IEEE Symp Business. Eng Ind Appl. <https://doi.org/10.1109/ISBEIA.2012.6422866>
50. Sharma M, Gaur A, Quamara JK (2020) Swift heavy ions irradiated PVDF/BaTiO₃ film as a separator for supercapacitors. Solid State Ionics 352:115342. <https://doi.org/10.1016/j.ssi.2020.115342>
51. Dutta B, Bose N, Kar E et al (2017) Smart, lightweight, flexible NiO/poly(vinylidene fluoride) nanocomposites film with significantly enhanced dielectric, piezoelectric and EMI shielding properties. J Polym Res 24:220. <https://doi.org/10.1007/s10965-017-1396-z>
52. Thakur P, Kool A, Bagchi B et al (2015) The role of cerium(III)/yttrium(III) nitrate hexahydrate salts on electroactive β phase nucleation and dielectric properties of poly(vinylidene fluoride) thin films. RSC Adv 5:28487–28496. <https://doi.org/10.1039/c5ra03524d>
53. Rajeh A, Althobaiti HA, Almeahmadi SJ et al (2023) Alteration in the Structural, Optical, Thermal, Electrical, and Dielectric properties of PMMA/PVDF blend by Incorporation of Ni/ZnO Nanohybrid for Optoelectronic and Energy Storage Devices. J Inorg Organomet Polym Mater. <https://doi.org/10.1007/s10904-023-02880-w>
54. Sharma M, Gaur A (2021) Fabrication of PVDF/BaTiO₃/NiO nanocomposite film as a separator for supercapacitors. J Energy Storage 38:102500. <https://doi.org/10.1016/j.est.2021.102500>
55. Mohanty HS, Ravikant, Kumar A et al (2019) Dielectric/ferroelectric properties of ferroelectric ceramic dispersed poly(vinylidene fluoride) with enhanced β -phase formation. Mater Chem Phys 230:221–230. <https://doi.org/10.1016/j.matchemphys.2019.03.055>
56. Martins P, Lopes AC, Lanceros-Mendez S (2014) Electroactive phases of poly(vinylidene fluoride): determination, processing and applications. Prog Polym Sci 39:683–706. <https://doi.org/10.1016/j.progpolymsci.2013.07.006>
57. Paul BK, Mondal D, Das S et al (2018) Iron-Doped, Mullite-Impregnated PVDF Composite: An Alternative Separator for a High Charge Storage Ceramic Capacitor. J. Electron. Mater. 47:7075–7084. <https://doi.org/10.1007/s11664-018-6635-5>
58. Zhu L, Wang Q (2012) Novel ferroelectric polymers for high energy density and low loss dielectrics. Macromolecules 45:2937–2954. <https://doi.org/10.1021/ma2024057>
59. Karasawa N, Goddard WA, Field IIF (1992) fi 5:7268–7281
60. Hoque NA, Thakur P, Roy S et al (2017) Er³⁺/Fe³⁺ + stimulated Electroactive, visible light emitting, and high dielectric flexible PVDF Film Based Piezoelectric nanogenerators: a simple and Superior Self-Powered Energy Harvester with Remarkable Power Density. ACS Appl Mater Interfaces 9:23048–23059. <https://doi.org/10.1021/acsami.7b08008>
61. Sutradhar S, Saha P, Chowdhury A, Das S (2019) Reduction of electromagnetic pollution by the enhancement of microwave absorption of strontium hexaferrite functionalized poly(vinylidene fluoride) composite film. Mater Res Express 6:086424. <https://doi.org/10.1088/2053-1591/ab1ab2>
62. S. Sutradhar, S. Saha, S. Javed, Shielding Effectiveness Study of Barium Hexaferrite-Incorporated, β -Phase-Improved Poly(vinylidene fluoride) Composite Film: A Metamaterial Useful for the Reduction of Electromagnetic Pollution (2019) ACS Appl. Mater. Interfaces 11(26):23701–23713. <https://doi.org/10.1021/acsami.9b05122>
63. Chakraborty T, Sharma S, Ghosh A et al (2020) Electromagnetic shielding effectiveness of X-Type Hexaferrite-C₃N₄ Binary Nanofiller-Incorporated Poly(vinylidene fluoride) multiphase composites. J Phys Chem C 124:19396–19405. <https://doi.org/10.1021/acs.jpcc.0c05666>
64. Sizochenko N, Mikolajczyk A, Syzochenko M et al (2021) Zeta potentials (ζ) of metal oxide nanoparticles: a meta-analysis of experimental data and a predictive neural networks modeling. NanoImpact 22:100317. <https://doi.org/10.1016/j.impact.2021.100317>
65. Iqbal J, Abbasi BA, Ahmad R et al (2020) Phyto-genic synthesis of nickel oxide nanoparticles (NiO) using fresh leaves extract of Rhamnus Triquetra (Wall.) And investigation of its multiple in vitro biological potentials. Biomedicines 8. <https://doi.org/10.3390/BIOMEDICINES8050117>
66. Toropov AA, Sizochenko N, Toropova AP, Leszczynski J (2018) Towards the development of global nano-quantitative structure–property relationship models: Zeta potentials of metal oxide nanoparticles. Nanomaterials. <https://doi.org/10.3390/nano8040243>
67. Chen S, Chen S, Qiao R et al (2021) Enhanced dielectric constant of PVDF-based nanocomposites with one-dimensional core-shell polypyrrole/sepiolite nanofibers. Compos Part Appl Sci Manuf 145:106384. <https://doi.org/10.1016/j.compositesa.2021.106384>
68. Gebrekrstos A, Muzata TS, Ray SS (2022) Nanoparticle-enhanced β -Phase formation in Electroactive PVDF composites: a review of systems for Applications in Energy Harvesting, EMI shielding, and membrane technology. ACS Appl Nano Mater 5:7632–7651. <https://doi.org/10.1021/acsnm.2c02183>
69. Dhatarwal P, Sengwa RJ (2019) Impact of PVDF/PEO blend composition on the β -phase crystallization and dielectric properties of silica nanoparticles incorporated polymer nanocomposites. J Polym Res 26:196. <https://doi.org/10.1007/s10965-019-1859-5>
70. El-Kemary M, Nagy N, El-Mehasseb I (2013) Nickel oxide nanoparticles: synthesis and spectral studies of interactions with glucose. Mater Sci Semicond Process 16:1747–1752. <https://doi.org/10.1016/j.mssp.2013.05.018>
71. Kar E, Bose N, Dutta B et al (2019) Ultraviolet-and Microwave-Protecting, Self-Cleaning e-Skin for efficient energy harvesting and Tactile Mechanosensing. ACS Appl Mater Interfaces 11:17501–17512. <https://doi.org/10.1021/acsnami.9b06452>
72. Bhatt AS, Bhat DK (2012) Influence of nanoscale NiO on magnetic and electrochemical behavior of PVDF-based polymer nanocomposites. Polym Bull 68:253–261. <https://doi.org/10.1007/s00289-011-0628-3>
73. Ai L, Fang G, Yuan L et al (2008) Influence of substrate temperature on electrical and optical properties of p-type semitransparent conductive nickel oxide thin films deposited by radio frequency sputtering. Appl Surf Sci 254:2401–2405. <https://doi.org/10.1016/j.apsusc.2007.09.051>
74. Biswas P, Hoque NA, Thakur P et al (2019) Highly efficient and Durable Piezoelectric Nanogenerator and Photo-power cell based on CTAB Modified Montmorillonite Incorporated PVDF Film. ACS Sustain Chem Eng 7:4801–4813. <https://doi.org/10.1021/acssuschemeng.8b05080>
75. Li H, Zhang Q, Chong C et al (2019) Ac Ce pte d M us pt. Mater Today Proc 22:16–20
76. Theerthagiri J, Senthil RA, Buraidah MH et al (2015) Effect of tetrabutylammonium iodide content on PVDF-PMMA polymer blend electrolytes for dye-sensitized solar cells. Ionics (Kiel) 21:2889–2896. <https://doi.org/10.1007/s11581-015-1464-5>
77. Liu F, Li Z, Wang Q, Xiong C (2018) High breakdown strength and low loss binary polymer blends of poly(vinylidene fluoride)-trifluoroethylene-chloroethoxyethylene and poly(methyl methacrylate). Polym Adv Technol 29:1271–1277. <https://doi.org/10.1002/pat.4238>
78. Mondal I, Halder P, Kundu M, Paul BK, Biswas S, Pal A, Sau S, Mondal D, Paul PK, Das S (2024) Energy-efficient sintering-free Chemically synthesized carbon nanofibers for high-performance supercapacitors. Materials Today Chemistry 35:101905. <https://doi.org/10.1016/j.mtchem.2024.101905>
79. Manuscript A (1972) Dalton transactions. J Chem Soc Dalton Trans. <https://doi.org/10.1039/D4DT00166D>

80. Pervaiz S, Kanwal N, Hussain SA et al (2021) Study of structural, optical and dielectric properties of ZnO/PVDF-based flexible sheets. *J Polym Res* 28:309. <https://doi.org/10.1007/s10965-021-02640-9>
81. Cao D, Zhou W, Li T et al (2021) Tailoring dielectric performance of Ni/poly(vinylidene fluoride) composites through constructing NiO shell as an interlayer. *J Polym Res* 28:14–16. <https://doi.org/10.1007/s10965-021-02594-y>
82. Devi PI, Ramachandran K (2011) Dielectric studies on hybridised PVDF – ZnO nanocomposites. 8080. <https://doi.org/10.1080/17458080.2010.497947>
83. Sahoo R, Mishra S, Ramadoss A et al (2020) Temperature-dependent dielectric properties of metal-doped ZnO nanofiller reinforced PVDF nanocomposites. *Mater Res Bull* 132:111005. <https://doi.org/10.1016/j.materresbull.2020.111005>
84. Sahoo R, Mishra S, Unnikrishnan L et al (2020) Enhanced dielectric and piezoelectric properties of Fe-doped ZnO/PVDF-TrFE composite films. *Mater Sci Semicond Process* 117:105173. <https://doi.org/10.1016/j.mssp.2020.105173>

Publisher's Note Springer Nature remains neutral with regard to jurisdictional claims in published maps and institutional affiliations.

Springer Nature or its licensor (e.g. a society or other partner) holds exclusive rights to this article under a publishing agreement with the author(s) or other rightsholder(s); author self-archiving of the accepted manuscript version of this article is solely governed by the terms of such publishing agreement and applicable law.